References

1 ARAKAWA, Y., VAHALA, K., and YARIV, A.: 'Quantum noise and dynamics in quantum well and quantum wire lasers', *Appl. Phys. Lett.*, 1984, **45**, pp. 950–952

2 SUEMUNE, I., COLDREN, L. A., YAMANISHI, M., and KAN, Y.: 'Extremely wide modulation bandwidth in a low threshold current strained quantum well laser', *Appl. Phys. Lett.*, 1988, **53**, pp. 1378–380

3 FUKUSHIMA, T., BOWERS, J. E., LOGAN, R. A., TANBUN-EK, T., and TEMKIN, H.: 'Effect of strain on the resonant frequency and damping factor in InGaAs/InP multiple quantum well lasers', *Appl. Phys. Lett.*, **58**, pp. 1244–1246

4 LEALMAN, I. F., BAGLEY, M., COOPER, D. M., FLETCHER, N., HARLOW, M., PERRIN, S. D., WALLING, R. H., and WESTBROOK, L. D.: 'Wide bandwidth multiple quantum well 1·55 μm lasers', *Electron. Lett.*, 1991, **27**, pp. 1191–1193

5 MATTHEWS, J. W., and BLAKESLEE, A. E.: 'Defects in epitaxial multilayers', *J. Cryst. Growth*, 1974, **27**, pp. 118–125

6 SELTZER, C. P., PERRIN, S. D., TATHAM, M. C., and COOPER, D. M.: 'Zero-net-strain multiquantum well lasers', *Electron. Lett.*, 1991, **27**, pp. 1268–1269

7 SELTZER, C. P., BURNESS, A. L., STEVENSON, M., HARLOW, M. J., COOPER, D. M., REDSTALL, R. M., and SPURDENS, P. C.: 'Reliable 1·5 μm buried heterostructure separate confinement, multiple quantum well (BH-SC-MQW) lasers entirely grown by metalorganic vapour phase epitaxy (MOVPE)', *Electron. Lett.*, 1989, **25**, pp. 1449–1450

8 ADAMS, A. R.: 'Band-structure engineering for low-threshold high-efficiency semiconductor lasers', *Electron. Lett.*, 1986, **22**, pp. 249–250

9 TATHAM, M. C., LEALMAN, I. F., SELTZER, C. P., WESTBROOK, L. D., and COOPER, D. M.: 'Resonance frequency, damping and differential gain in 1·55 μm multiple quantum well lasers', to be published in *IEEE J. Quantum Electron.*

CODING TO INCREASE NUMBER OF CHANNELS IN QAM-SCM-IM/DD LIGHTWAVE SYSTEM

J.-H. Wu, Y.-H. Lee and J. Wu

Indexing terms: Optical communication, Television, Optical modulation

For a fibre-optic QAM-SCM-IM/DD system, clipping noise can severely limit the channel transport capability. A theoretical analysis of the QAM-SCM-IM/DD system employing BCH codes to increase the number of channels is presented. The relations among the system parameters such as received signal power, modulation index, and carrier-to-noise ratio are investigated. A general expression of the number of channels in terms of these parameters is also presented. The example shows that by using a (255, 239) BCH code, the number of channels can be increased up to fivefold, and the influence of clipping noise can also be greatly reduced.

Introduction: Recently, high-definition television (HDTV) has attracted much attention. Fully digital HDTV, such as the Digicipher system, has some advantages and may be popular in the future [1]. However, the transmission capacity required for an uncompressed digital HDTV signal is about 1 Gbit/s. With sophisticated image-coding techniques, a transmission rate of about 150 Mbit/s is possible. Therefore, multistage digital modulation must be used to transmit such a signal in a currently assigned TV channel (6 MHz for NTSC). For a fibre-optic SCM (subcarrier multiplexed) system, the clipping noise which results from the laser intensity fluctuation is a major limit, hence the modulation index per channel and the total number of channels are restricted. With Gaussian approximation, we theoretically investigate the benefit of applying coding to a fibre-optic QAM-SCM-IM/DD (intensity modulation/direct detection) system. A general expression of the number of channels is derived in terms of carrier-to-noise ratio (CNR), receiver sensitivity, and code parameters. It is shown that coding can be used to effectively combat clipping noise, and thus more channels can be located in a given band.

System description and analysis: Consider a QAM-SCM-IM/DD system as shown in Fig. 1. The N channels are transmitted by their corresponding microwave subcarriers (f_1, ..., f_N) with QAM modulation scheme, and are combined to modulate the laser diode (intensity modulation). At the receiving end, the subcarrier signals are directly detected by a photodiode. The output of the photodiode is amplified by a low noise amplifier (LNA). The bandpass filter (BPF) is used to select the desired channel. The circuit following is a typical QAM demodulator.

The CNR for a specific channel at the output of the BPF is given by [2, 3]

$$CNR^{-1} = \frac{8kTFB/R_L}{m^2(RP_s)^2} + \frac{4eB}{m^2RP_s} + \frac{2(RIN)B}{m^2} + CIR^{-1} \quad (1)$$

where k is the Boltzmann constant, T is the absolute temperature (300 K), F is the electronic receiver amplifier noise figure, R_L is the photodiode load resistor with a nominal value 50 Ω, e is the electron charge, B is the bandwidth of the IF filter, RIN stands for the relative intensity noise (dB/Hz), CIR is the carrier-to-interference ratio resulting from clipping as [4]

$$CIR = \sqrt{(2\pi)} \cdot \frac{1 + 6\mu^2}{\mu^3} \cdot \exp\left(\frac{1}{2\mu^2}\right) \quad (2)$$

and

$$\mu = m\sqrt{(N/2)} \quad (3)$$

μ represents the total root mean square (RMS) modulation index, and m is the modulation index per channel.

(A) *Uncoded case:* For the system without coding, we can substitute eqn. 3 into eqn. 1 to obtain the CNR as

$$CNR^{-1} = \frac{8kTFB/R_L}{(RP_s)^2} \cdot \frac{N}{2\mu^2} + \frac{4eB}{RP_s} \times \frac{N}{2\mu^2} + \frac{(RIN)B}{\mu^2} \cdot N + CIR^{-1} \quad (4)$$

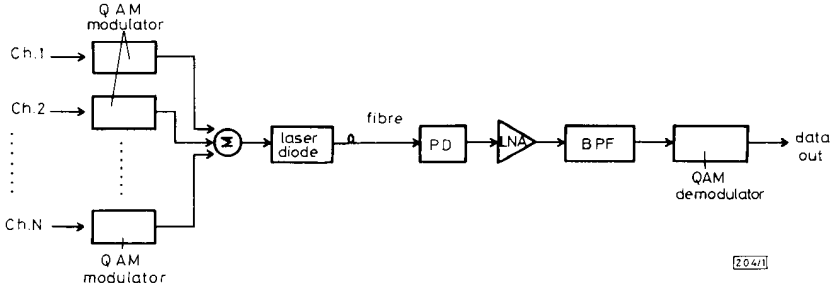

Fig. 1 *System block diagram of QAM-SCM-IM/DD system*

Solving eqn. 4 for N

$$N = (CNR^{-1} - CIR^{-1})\mu^2/A \tag{5}$$

where

$$A = \frac{4kTFB/R_L}{(RP_s)^2} + \frac{2eB}{RP_s} + (RIN)B \tag{6}$$

Substituting eqn. 2 into eqn. 5, we obtain

$$N = \left[CNR^{-1} \cdot \mu^2 - \frac{1}{\sqrt{(2\pi)}} \cdot \frac{\mu^5}{1 + 6\mu^2} \cdot \exp(-1/2\mu^2) \right] \Big/ A \tag{7}$$

Differentiating the right hand side of eqn. 7 with respect to μ and setting to zero, we obtain

$$CNR = 2\sqrt{(2\pi)} \cdot \frac{36\mu^4 + 12\mu^2 + 1}{18\mu^5 + 11\mu^3 + \mu} \cdot \exp(1/2\mu^2) \tag{8}$$

Substituting eqn. 8 into eqn. 7, the maximum value of N is

$$N_{uncoded} = \frac{(RP_s)^2 \cdot \exp(-1/2\mu^2)}{2\sqrt{(2\pi)}[4kTFB/R_L + (2eB) \times (RP_s) + (RIN)B(RP_s)^2]} \times \left(\frac{6\mu^7 + 9\mu^5 + \mu^3}{36\mu^4 + 12\mu^2 + 1} \right) \tag{9}$$

Using eqn. 3, we obtain the corresponding modulation index per channel as

$$m_{uncoded} = \sqrt{\left\{ 4\sqrt{(2\pi)} \left[\frac{4kTFB/R_L}{(RP_s)^2} + \frac{2eB}{RP_s} + (RIN)B \right] \times \left\{ \frac{36\mu^4 + 12\mu^2 + 1}{6\mu^5 + 9\mu^3 + \mu} \right) \exp(1/2\mu^2) \right\}} \tag{10}$$

(B) *Coded case:* In a coded system, suppose a code of rate r is used and the coding gain is G; then eqn. 4 can be modified as [5]

$$\left(\frac{CNR}{G}\right)^{-1} = \frac{8kTFB/(R_L r)}{(RP_s)^2} \cdot \frac{N}{2\mu^2} + \frac{4eB}{RP_s r} \times \frac{N}{2\mu^2} + \frac{(RIN)B}{\mu^2 r} \cdot N + CIR^{-1} \tag{11}$$

Similarly, we can solve eqn. 11 for N, and the following equation holds:

$$\frac{CNR}{G} = 2\sqrt{(2\pi)} \cdot \frac{36\mu^4 + 12\mu^2 + 1}{18\mu^5 + 11\mu^3 + \mu} \cdot \exp(1/2\mu^2) \tag{12}$$

so the maximum channel number of the coded system can be obtained as

$$N_{coded} = \frac{G}{2\sqrt{(2\pi)}} \times \frac{(RP_s)^2 r \cdot \exp(-1/2\mu^2)}{4kTFB/R_L + (2eB)(RP_s) + (RIN)B(RP_s)^2} \times \left(\frac{6\mu^7 + 9\mu^5 + \mu^3}{36\mu^4 + 12\mu^2 + 1} \right) \tag{13}$$

and the corresponding modulation index per channel is

$$m_{coded} = \sqrt{\left\{ \frac{4\sqrt{(2\pi)}}{Gr} \left[\frac{4kTFB/R_L}{(RP_s)^2} + \frac{2eB}{RP_s} + (RIN)B \right] \times \left(\frac{36\mu^4 + 12\mu^2 + 1}{6\mu^5 + 9\mu^3 + \mu} \right) \exp(1/2\mu^2) \right\}} \tag{14}$$

Numerical example: In the numerical example, we assume a 256 QAM-SCM-IM/DD system requiring a bit error rate (BER) of 10^{-9} and adopt the following parameters: $CNR = 39$ dB, $P_s = -12$ dBm, $R = 1$ A/W, $F = 3$ dB, and $RIN = -150$ dB/Hz. From eqn. 8, the required CNR against the total RMS modulation index is shown in Fig. 2. The value μ increases as the CNR decreases. Substituting the above parameters into eqns. 8 and 9, we obtain $\mu_{uncoded} = 0.29$, and $N_{uncoded} = 10$. By using a (255, 239) BCH code with a coding gain of 3.5 dB at $BER = 10^{-9}$ [6] ($G = 10^{0.35}$ and $r = 239/255$) in eqns. 12 and 13, we obtain $\mu_{coded} = 0.31$, and $N_{coded} = 52$.

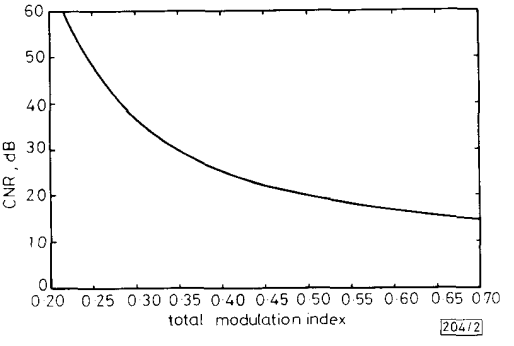

Fig. 2 *CNR value against total RMS modulation index μ*

Fig. 3 shows the number of channels against received signal power for the coded system and the uncoded system at $CNR = 39$ dB and $M = 256$. It is found that the channel number can be increased up to fivefold under the same receiver sensitivity and BER.

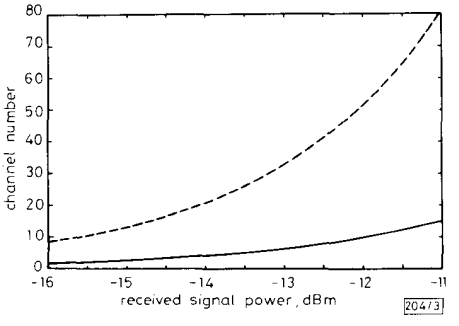

Fig. 3 *Channel number against received signal power for (255, 239) BCH coded and uncoded system at $CNR = 39$ dB, $M = 256$*

- - - - coded
——— uncoded

Conclusion: A general expression of a QAM-SCM-IM/DD system employing error control code to increase the number of channels is derived in terms of received signal power, carrier-to-noise ratio, and code parameters. As an example, by using a (255, 239) BCH code in a 256 system, the number of channels can be increased up to fivefold. Therefore, coding can be used to effectively combat clipping noise, and more channels can be located in a given band.

4th November 1991

J.-H. Wu, Y.-H. Lee and J. Wu (*Department of Electrical Engineering, National Taiwan University, Taipei, Taiwan 10764, Republic of China*)

References

1 PAIK, W.: 'Digicipher—all digital channel compatible, HDTV broadcast system', *IEEE Trans.*, 1990, **B-36**, (4), pp. 245–254
2 WAY, W. I.: 'Fiber-optic transmission of microwave 8-phase-PSK and 16-ary quadrature-amplitude-modulated signals at the 1·3 μm

wavelength region', *J. Lightwave Technol.*, 1988, **LT-8**, (2), pp. 273–280

3 KAVEHRAD, M., and SAVOY, E.: 'Fiber-optic transmission of microwave 64-QAM signals', *IEEE J. Sel. Areas Commun.*, 1990, **SAC-8**, (7), pp. 1320–1325

4 DARCIE, T. E.: 'Subcarrier multiplexing for lightwave networks and video distribution systems', *IEEE J. Sel. Areas Commun.*, 1990, **SAC-8**, (7), pp. 1240–1248

5 FOSCHINI, G. J., and SALEH, A. M.: 'Overcoming optical amplifier intermodulation distortion using coding in multichannel communications systems', *IEEE Trans.*, 1990, **COM-38**, (2), pp. 187–191

6 OHTSUKA, H., KAGAMI, O., KOMAKI, S., KOHIYAMA, K., and KAVEHRAD, M.: '256-QAM subcarrier transmission using coding and optical intensity modulation in distribution networks', *IEEE Photonics Technol. Lett.*, 1991, **3**, (4), pp. 381–383

ENERGY QUANTISATION IN FIGURE EIGHT FIBRE LASER

A. B. Grudinin, D. J. Richardson and D. N. Payne

Indexing terms: Lasers and laser applications, Nonlinear optics

For the first time the observation of discrete jumps in the power output of an all-fibre passively mode-locked laser is reported. The discontinuities are associated with quantisation of the energy of the pulses circulating within the laser cavity.

Introduction: The passive generation of femtosecond soliton pulses in erbium-doped fibre lasers has recently become of significant interest [1–3]. The figure eight laser configuration [2–4] whose operation is based on the reflection properties of the nonlinear amplifying loop mirror (NALM) [5] has been the object of considerable study and has so far been shown capable of generating bandwidth-limited pulses as short as 320 fs [2, 3]. In this scheme the quantisation of the soliton energy and the random nature of the pulse formation lead to several distinct regimes of pulse repetition rate behaviour [4]. In general, within one round trip period the solitons are randomly separated in time and the pulse trains repeat at the cavity round trip period. The exact pulse pattern and the total number of pulses in the cavity are highly sensitive to the input pump power. The repetition rate can be stabilised by incorporating a pulse multiplier into the cavity [6]; however, although the general principle of operation of the figure eight laser is understood, many features of its behaviour still remain to be investigated and explained.

We present for the first time experimental results showing the effects of pulse energy quantisation in the power output from the laser. The results demonstrate the preference of the laser to operate in well defined soliton units and its ability to adapt itself to changes of input pump power once soliton selfstarting has occurred.

Experiment: The experimental setup is shown in Fig. 1. The laser was configured to generate transform-limited, 450 fs soliton pulses at 1558 nm. The NALM loop was 35 m long and the cavity round trip frequency was 5 MHz. The amplifier section consisted of 3 m of 800 *ppm* erbium-doped fibre and was pumped by a Ti : sapphire laser operating at 980 nm. An acousto-optic modulator was placed in front of the 980 nm pump launch stabilisation circuitry, the 980 nm pump level to we were able to lock the input pump power to the figure-eight laser to an externally defined reference voltage. Thus by applying a slow sawtooth waveform (100 s period) to the pump launch stabilisation circuitry the 980 nm pump level to the laser could be controllably and repeatedly varied, while measuring the average output power at port 1 on a slow detector (light emanating at port 1 has been switched by the NALM and is the correct port for soliton output). The pulse repetition rate behaviour and optical spectra were simultanously measured at port 1. The same measurements could also be made at port 2 where light reflected by the NALM (i.e. the nonsolitonic component) can be observed.

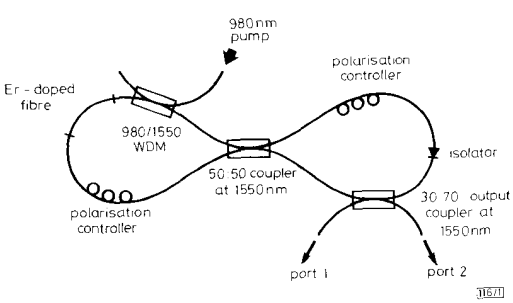

Fig. 1 *Experimental configuration*

A typical laser output characteristic measured at port 1 is shown in Fig. 2 and exhibits a number of interesting features, such as discrete jumps and hysteresis in the output power. The CW lasing threshold is seen to occur at approximately 10 mW, whereas a 'second threshold' occurs at around 45 mW, where soliton modelocked operation selfstarts. Once pulsed operation initiates it can be sustained at reduced pump power levels, down to within a few milliwatts of the CW laser threshold, giving rise to a hysteresis in the power output.

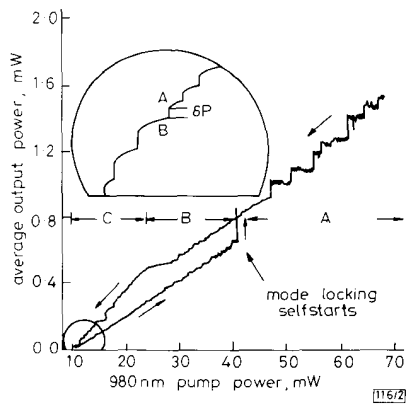

Fig. 2 *Typical laser characteristic*

Inset: output power, on an expanded scale, at low values of input pump power (Note: inset laser characteristic corresponds to another hysteresis measurement from small scale curve)

In the time domain, three regions of pulsed operation can be identified, corresponding to regions A–C on the laser output characteristic (Fig. 2).

(i) *Region A:* For pump powers above the mode-locking self-start threshold, many pulses exist within the laser resonator. The pulses undergo complicated motions with respect to each other, possibly due to soliton–soliton interactions. Owing to the random nature of the laser pulsing, the pulse patterns and motions vary with time and the detailed features of the laser characteristic similarly differ for each sweep of the pump power. A small CW component is also apparent.

(ii) *Region B:* As the pump power is lowered below the self-starting threshold the pulse motions become progressively less chaotic and the laser output smoother until, at a power level of 25 mW, the output power curve displays a distinct hump.

(iii) *Region C:* The laser slope efficiency is increased below the output characteristic hump. In the time domain the pulses group themselves into ordered patterns and all motions cease (see Fig. 3). The small accompanying CW level at the output noted at higher pump powers also disappears. As the pump power is further reduced abrupt jumps (inset Fig. 2) in output power are observed and are associated with the disappearance